



Transverse spinning of unpolarized light

J. S. Eismann^{1,2,3,9}, L. H. Nicholls^{4,9}, D. J. Roth^{4,9}, M. A. Alonso^{5,6}, P. Banzer^{1,2,3}✉,
F. J. Rodríguez-Fortuño⁴, A. V. Zayats⁴✉, F. Nori^{7,8} and K. Y. Bliokh⁷✉

It is well known that the spin angular momentum of light, and therefore that of photons, is directly related to their circular polarization. Naturally, for totally unpolarized light, polarization is undefined and the spin vanishes. However, for non-paraxial light, the recently discovered transverse spin component, orthogonal to the main propagation direction, is largely independent of the polarization state of the wave. Here, we demonstrate, both theoretically and experimentally, that this transverse spin survives even in non-paraxial fields (for example, focused or evanescent) generated from totally unpolarized paraxial light. This counterintuitive phenomenon is closely related to the fundamental difference between the meanings of ‘full depolarization’ for two-dimensional (2D) paraxial and 3D non-paraxial fields. Our results open an avenue for studies of spin-related phenomena and optical manipulation using unpolarized light.

Classical polarization optics usually examines paraxial light and its two-dimensional (2D) polarization states¹. Similarly, the spin of photons in quantum electrodynamics textbooks is also described by 2D circular polarizations of plane electromagnetic waves². However, modern nano-optics is based on the use of structured non-paraxial fields, where all three spatial components of the field vector generically play a role³. This has required extending existing polarization theory to the 3D case^{4–12}. This extension is by no means trivial, with the four Stokes parameters describing generic 2D polarization being substituted by nine polarization parameters characterizing generic 3D polarization.

Simultaneously, the notion of spin has had to be augmented to 3D structured fields^{13–17}. The local spin density is well defined for monochromatic waves and can be associated with the radiation torque on small dipole particles¹⁷. This has led to the discovery of the unusual transverse spin in inhomogeneous fields, which has several remarkable properties^{18–32} (for reviews, see refs. ^{17,33–35}). This spin, orthogonal to the main propagation direction and wavevectors, is a very robust phenomenon that has found applications for spin-direction coupling using evanescent waves, which is highly efficient and largely independent of the details of the system^{22–25,27–29,33–35}. Moreover, it was recently found that the transverse spin is equally present in inhomogeneous sound waves^{36–38} (which are traditionally considered to be scalar, that is, spinless), quantum electron waves²⁹ and even gravitational waves³⁹.

In this Article, we demonstrate, both theoretically and experimentally, that the transverse spin is essentially a 2D-polarization-independent phenomenon, which survives even in 3D fields generated from totally unpolarized paraxial light (Fig. 1). This is in sharp contrast to the usual longitudinal spin, which is directly related to the 2D polarization and vanishes in unpolarized fields. We show that this phenomenon is intimately related to the difference between the 2D and 3D polarization descriptions. Namely, the totally unpolarized 2D field is, at the same time, half-polarized in the 3D sense (according to the definition⁵). Indeed, 2D depolarization implies a single random phase between the two orthogonal field components

(with equal amplitudes), while complete 3D depolarization requires two random phases between the three mutually orthogonal field components. Therefore, any regular optical transformation producing a non-paraxial 3D field from a 2D-unpolarized far-field source will have partial 3D polarization, with the degree of polarization not less than 1/2. In particular, a local increase of the degree of polarization up to almost 1 has been demonstrated for the tight focusing of an unpolarized paraxial beam^{40,41}. In the following, we show that the transverse spin appears in any paraxial-to-non-paraxial transformation (Fig. 1), even without a change in the degree of polarization. The minimal value of 1/2 allows for non-zero spin in such fields. The origin of this phenomenon lies in the intrinsic spin-orbit interaction of light³⁴, where any transformation in the wavevector direction produces spin-related phenomena, even for 2D-unpolarized light.

Because spin is a fundamental dynamical property of light, which is very important in both quantum and classical theoretical and applied optics (for example, for optical manipulation of micro- and nanoparticles), our findings provide a novel opportunity to use polarization-independent spin from unpolarized sources.

Theoretical background

Non-paraxial optical fields are usually generated from far-field sources of paraxial light via some optical transformations (Fig. 1): focusing, diffraction, scattering and so on. In this Article, we consider two of the most common examples of non-paraxial fields: (1) tightly focused Gaussian-like beams and (2) evanescent waves. These are generated via high-numerical-aperture (NA) focusing and total internal reflection of the incident paraxial light, respectively.

The incident paraxial light can be approximated by a plane wave, so its 2D polarization state can be described by the 2×2 polarization (density) matrix $\hat{\Phi}^{2D}$ or, equivalently, by four real Stokes parameters $\vec{s} = (s_0, s_1, s_2, s_3)$, where $\hat{\Phi}^{2D} = \frac{1}{2} \sum_{l=0}^3 s_l \hat{\sigma}_l$, with $\hat{\sigma}_l$ being the basic Pauli matrices¹. Here, the normalized parameter s_3 corresponds to the normalized spin angular momentum density of the wave (z-directed along the wave propagation), $S_z/I = s_3/s_0 \in [-1, 1]$

¹Max Planck Institute for the Science of Light, Erlangen, Germany. ²Institute of Optics, Information, and Photonics, University Erlangen-Nuremberg, Erlangen, Germany. ³Institute of Physics, University of Graz, NAWI Graz, Graz, Austria. ⁴Department of Physics and London Centre for Nanotechnology, King's College London, London, UK. ⁵CNRS, Centrale Marseille, Institut Fresnel, Aix Marseille Univ., Marseille, France. ⁶The Institute of Optics, University of Rochester, Rochester, NY, USA. ⁷Theoretical Quantum Physics Laboratory, RIKEN Cluster for Pioneering Research, Saitama, Japan. ⁸Physics Department, University of Michigan, Ann Arbor, MI, USA. ⁹These authors contributed equally: J. S. Eismann, L. H. Nicholls, D. J. Roth. ✉e-mail: Peter.banzer@uni-graz.at; a.zayats@kcl.ac.uk; k.bliokh@gmail.com

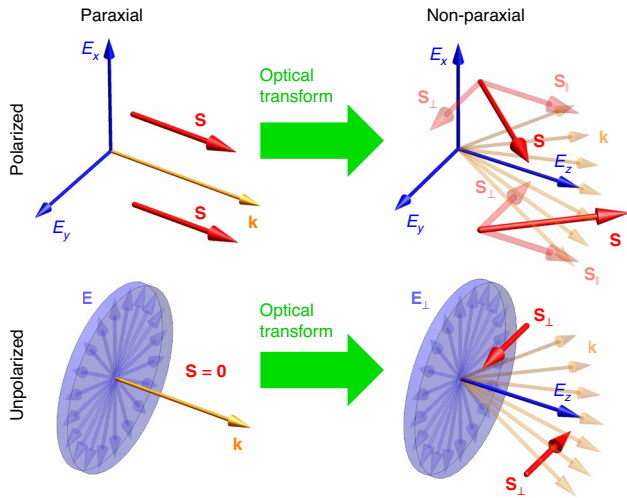


Fig. 1 | Spin and polarization in paraxial and non-paraxial fields. Schematic of the longitudinal and transverse spin for the paraxial (plane-wave) and non-paraxial regimes for polarized and unpolarized (in the two-dimensional (2D) sense) fields. Transverse spin \mathbf{S}_\perp appears in non-paraxial fields, while the depolarization of the paraxial source eliminates only the longitudinal spin \mathbf{S}_\parallel .

(ref. ¹⁷), where $I = W/\omega$ is the wave intensity expressed via the energy density W and frequency ω . The degree of paraxial 2D polarization is defined as $P^{2D} = \sqrt{\sum_{i=1}^3 s_i^2/s_0} \in [0, 1]$. For totally 2D-unpolarized light, $\vec{s} \propto (1, 0, 0, 0)$, $P^{2D} = 0$, and the spin vanishes: $S_z = 0$ (Fig. 1).

For the generated non-paraxial field, all three components are significant, and its polarization state at a point is described by a 3×3 Hermitian polarization (density) matrix $\hat{\Phi}^{3D}$ or, equivalently, by nine real parameters $\vec{\Lambda} = (\Lambda_0, \Lambda_1, \dots, \Lambda_8)$: $\hat{\Phi}^{3D} = \frac{1}{2} \sum_{l=0}^8 \Lambda_l \hat{\lambda}_l$, with $\hat{\lambda}_l$ being the basic Gell–Mann matrices^{4–12} (Supplementary Information). In such fields, the polarization ellipsoid can have an arbitrary orientation, and the spin angular momentum density involves all three components^{14,17}. Its normalized value can be expressed via the properly normalized parameters Λ_2, Λ_5 and Λ_7 (Supplementary Information):

$$\frac{\mathbf{S}}{I} \equiv \frac{1}{I} (S_x, S_y, S_z) = \frac{2}{3\Lambda_0} (-\Lambda_7, \Lambda_5, -\Lambda_2). \quad (1)$$

There are several quantities characterizing the degree of polarization of a 3D field, which can be more or less relevant to the particular problem^{4–12}. In our case, one of the most common definitions of the 3D degree of polarization is useful— $P^{3D} = \sqrt{\sum_{i=1}^8 \Lambda_i^2} / \sqrt{3\Lambda_0} \in [0, 1]$ (refs. ^{5,10–12,40,41})—because it explicitly involves the norm of the spin given by equation (1), so that $(P^{3D})^2$ is a sum of spin-dependent and spin-independent parts. For a totally unpolarized 3D field, one should expect $\vec{\Lambda} \propto (1, 0, 0, \dots, 0)$, $P^{3D} = 0$ and the corresponding vanishing spin $\mathbf{S} = \mathbf{0}$.

One remarkable feature of the above definition of the degree of polarization is that totally 2D-unpolarized paraxial light, $P^{2D} = 0$, is partially polarized in the 3D sense, $P^{3D} = 1/2$ (refs. ^{5,11,12} and Supplementary Information). This is because total 3D depolarization requires total mutual decoherence of all three field components with equal amplitudes, while in paraxial light, the longitudinal z component vanishes. As a result, $\Lambda_8 = (\sqrt{3}/2)\Lambda_0 \neq 0$, even for a totally 2D-unpolarized paraxial field. This ‘discrepancy’ between

the 2D and 3D polarization degrees naturally manifests itself as a non-zero transverse spin in a non-paraxial field generated from a 2D-unpolarized paraxial source (Fig. 1).

We first consider the case of a focused polarized field. Both the incident paraxial and focused non-paraxial fields can be modelled by the post-paraxial description of a Gaussian beam¹⁷, with infinite and finite Rayleigh range z_R , respectively. Using the natural cylindrical coordinates (r, φ, z) , the normalized spin density in the focal plane of a polarized Gaussian beam can be written as (Supplementary Information)

$$\frac{\mathbf{S}}{I} \simeq \frac{1}{1 + \tilde{r}^2/2} \left[\frac{\mathbf{S}_0}{I_0} + \tilde{r} \vec{\Phi} \right] \equiv \frac{\mathbf{S}_\parallel}{I} + \frac{\mathbf{S}_\perp}{I}. \quad (2)$$

Here, $\mathbf{S}_0/I_0 = (s_3/s_0)\vec{z}$ is the spin density in the plane-wave limit, $I \propto (1 + \tilde{r}^2/2)e^{-k\tilde{r}^2/z_R}$ is the intensity distribution, k is the wavenumber, $\tilde{r} = r/z_R$, and the overbars indicate the unit vectors of the corresponding axes. Equation (2) exhibits the usual polarization-dependent longitudinal spin, as well as the transverse spin component^{17,26,32,33}, which is independent of the polarization (Stokes parameters) of the incident plane wave.

The totally 2D-unpolarized Gaussian beam can be considered as an incoherent superposition of two Gaussian beams with mutually orthogonal polarization states (for example, with $\vec{s} \propto (1, 1, 0, 0)$ and $\vec{s} \propto (1, -1, 0, 0)$). The corresponding 3×3 polarization matrix and parameters $\vec{\Lambda}$ in the focal plane of such unpolarized Gaussian field become (Supplementary Information): $\Lambda_1 = \Lambda_2 = \Lambda_3 = \Lambda_4 = \Lambda_6 = 0$,

$$\frac{\Lambda_8}{\Lambda_0} \simeq \frac{\sqrt{3}}{2} \frac{1 - \tilde{r}^2}{1 + \tilde{r}^2/2}, \quad \frac{\Lambda_5}{\Lambda_0} \simeq \frac{3}{2} \frac{\tilde{x}}{1 + \tilde{r}^2/2}, \quad \frac{\Lambda_7}{\Lambda_0} \simeq \frac{3}{2} \frac{\tilde{y}}{1 + \tilde{r}^2/2}, \quad (3)$$

where $\tilde{x} = x/z_R$ and $\tilde{y} = y/z_R$. In the paraxial limit $z_R \rightarrow \infty$, only the Λ_8/Λ_0 ratio survives, providing the 3D degree of polarization $P^{3D} = 1/2$ (refs. ^{5,11,12}). In the non-paraxial case, non-zero parameters Λ_5 and Λ_7 appear. These parameters exactly describe the transverse part of spin (2), in agreement with equation (1), $\mathbf{S}_\perp/I = \frac{2}{3\Lambda_0} (-\Lambda_7, \Lambda_5, 0)$, while the longitudinal spin naturally vanishes: $\mathbf{S}_\parallel = \mathbf{0}$ (Fig. 1).

We next consider an evanescent wave, which can be generated via total internal reflection of a paraxial incident field (plane wave). Such a z -propagating and x -decaying wave is characterized by the propagation constant $k_z > k \equiv \omega/c$ and the decay constant $\kappa = \sqrt{k_z^2 - k^2}$. Assuming, for simplicity, that the transmission coefficients of the total internal reflection are polarization-independent, generation of the evanescent field can be regarded as a transition from the plane-wave limit $\kappa = 0$, $k_z = k$ to a given finite $\kappa > 0$. The normalized spin density of the polarized evanescent wave is^{17,20}

$$\frac{\mathbf{S}}{I} = \frac{k}{k_z} \frac{\mathbf{S}_0}{I_0} + \frac{\kappa}{k_z} \vec{y} \equiv \frac{\mathbf{S}_\parallel}{I} + \frac{\mathbf{S}_\perp}{I}. \quad (4)$$

Here, as before, $\mathbf{S}_0/I_0 = (s_3/s_0)\vec{z}$ is the spin density in the plane-wave limit, and the intensity distribution is $I \propto e^{-2\kappa x}$. As for the focused field, the spin (4) consists of the longitudinal polarization-dependent component and the transverse (y -directed) polarization-independent term^{17,20,29,33,34}.

The totally 2D-unpolarized evanescent field is obtained as an incoherent superposition of evanescent waves with orthogonal polarization states. The corresponding parameters $\vec{\Lambda}$ for such an evanescent field are (Supplementary Information): $\Lambda_1 = \Lambda_2 = \Lambda_4 = \Lambda_6 = \Lambda_7 = 0$,

$$\frac{\Lambda_8}{\Lambda_0} = \frac{\sqrt{3}}{2} \frac{k^2 - \kappa^2}{k_z^2}, \quad \frac{\Lambda_3}{\Lambda_0} = \frac{3\kappa^2}{4k_z^2}, \quad \frac{\Lambda_5}{\Lambda_0} = \frac{3\kappa}{2k_z} \quad (5)$$

In the plane-wave limit $\kappa = 0$, only the ratio Λ_8/Λ_0 survives, yielding $P^{3D} = 1/2$. In the evanescent-wave case, both Λ_3 and Λ_5 are different

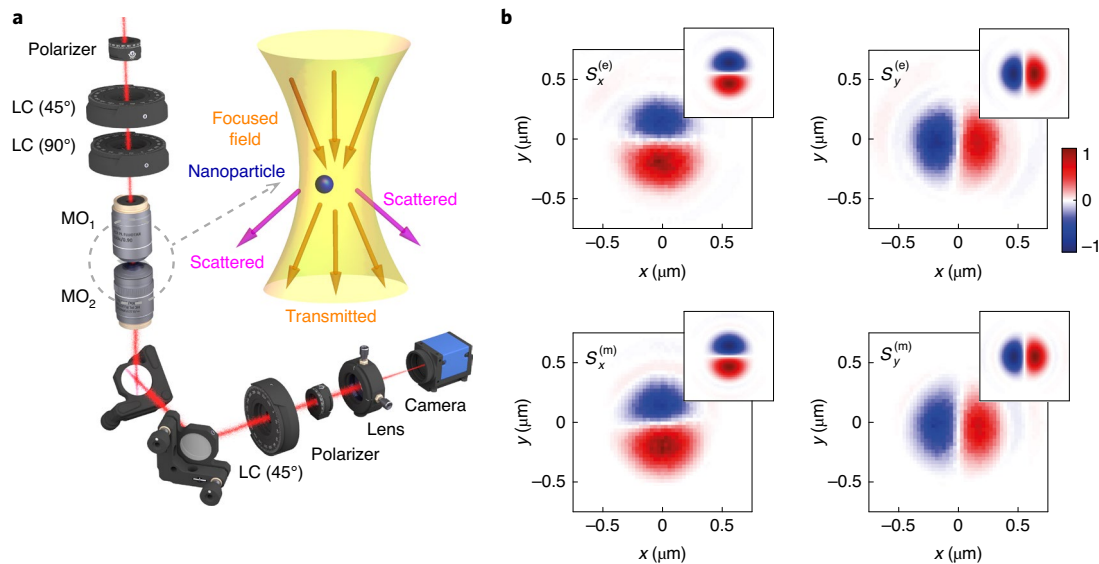


Fig. 2 | Focused-beam experiment. **a**, Experimental set-up for the reconstruction of the transverse spin in a tightly focused 2D-unpolarized field. A linear polarizer and two liquid-crystal variable retarders (LCs) are used to prepare a beam with randomly varied polarization. Subsequently, two confocally aligned microscope objectives (MOs) focus and collimate the beam. A spherical silicon nanoparticle is placed on a coverslip in the focal plane. This produces scattered light with wavevectors outside of the aperture of the transmitted beam, which carries information about the local transverse spin density in the beam^{26,32}. Polarization-resolved back focal plane images using the scattered light are recorded by using another LC, a linear polarizer and a lens. **b**, Experimental results of the reconstructed electric and magnetic transverse spin, $\mathbf{S}_{\perp}^{(e)}$ and $\mathbf{S}_{\perp}^{(m)}$ (normalized to the maximum absolute value), which equal each other in the 2D-unpolarized field (Supplementary Information). The results of numerical calculations are shown as insets.

from zero, the latter corresponding precisely to the transverse part of spin (4), in agreement with equation (1), $\mathbf{S}_{\perp}/I = \frac{2}{3\Lambda_0}(-\Lambda_7, \Lambda_5, -\Lambda_2)$, whereas the longitudinal spin vanishes, $\mathbf{S}_{\parallel} = \mathbf{0}$ (Fig. 1).

Importantly, considering r/z_R and κ/k as a small parameter ϵ in the above two problems, the 3D degree of polarization of the 2D-unpolarized focused and evanescent fields has the form $P^{3D} = \frac{1}{2} + \delta P^{3D}$, with $\delta P^{3D} \sim \epsilon^2$ and $\delta P^{3D} \sim \epsilon^4$, respectively (Supplementary Information), while the transverse spin is of order ϵ . This means that, to first order, focusing or total-reflection processes (with polarization-independent transmission amplitudes) do not change the 3D degree of polarization of the incident 2D-unpolarized light^{40,41}, while the spin changes from zero in the incident wave to the non-zero transverse spin in the non-paraxial field. This appearance of spin without polarization originates from the intrinsic spin-orbit interaction of light³⁴. The plane-wave transversality condition $\mathbf{k} \cdot \mathbf{E} = \mathbf{k} \cdot \mathbf{H} = 0$ imposes constraints on the relations between longitudinal and transverse field components, which therefore have some intrinsic mutual coherence even for fields generated from 2D-unpolarized sources. Transformations from paraxial to non-paraxial fields can be approximated by \mathbf{k} -vector transformations (redirections), which do not affect the degree of polarization but inevitably generate the transverse spin, as schematized in Fig. 1.

Another important point in our calculations is that we considered both electric and magnetic field contributions to all quadratic quantities (Supplementary Information): spin $\mathbf{S} = \mathbf{S}^{(e)} + \mathbf{S}^{(m)}$, intensity $I = I^{(e)} + I^{(m)}$, polarization parameters $\vec{\Lambda} = \vec{\Lambda}^{(e)} + \vec{\Lambda}^{(m)}$ and so on. For polarized fields, the electric and magnetic contributions are not equal to each other, and additional terms generally appear when considering only the electric or the magnetic fields^{17,20,26,32}. By contrast, for 2D-unpolarized fields, these contributions are always equal to each other, so that one can only consider the electric (or magnetic) field contributions. One can say that unpolarized light and its transverse spin have a dual-symmetric nature^{16,42}, similar to circularly polarized fields with well-defined helicity¹⁵.

In what follows, we present experimental measurements of the non-zero transverse spin from equations (2) and (4) in tightly focused and evanescent fields generated from 2D-unpolarized sources. The two experiments use different types of unpolarized sources and measure both the electric and magnetic contributions to the spin.

Focused-beam experiment

To measure the transverse spin of a 2D-unpolarized tightly focused beam, we first prepared a suitable input field. We sent a Gaussian beam (wavelength $\lambda = 2\pi/k = 620$ nm, linewidth $\Delta\lambda_{FWHM} \simeq 5$ nm) through a linear polarizer and two liquid-crystal variable retarders (LCs) oriented at 45° and 90° with respect to the axis of the linear polarizer, respectively. A schematic of the experimental set-up is shown in Fig. 2a^{32,43}. With this arrangement, the polarization state of the generated beam can span the whole Poincaré sphere ($\sum_{i=1}^3 s_i^2 = s_0^2$), with the position on the sphere depending on the settings of the LCs. These LCs were controlled via a voltage applied to the corresponding devices to induce a voltage-dependent birefringence. For the applied voltage, we used two random numbers in a range spanning multiple wavelengths of retardance, updated 10 times per second. This produced a beam that is fully and homogeneously polarized over its cross-section for a fixed instance in time. However, the beam appears totally 2D-unpolarized ($P^{2D} = \sum_{i=1}^3 s_i^2 = 0$) when averaged over a certain time frame.

For tight focusing and subsequent collimation of the light beam, we used two confocally aligned microscope objectives (MOs) with numerical apertures $NA_1 = 0.9$ and $NA_2 = 1.3$, respectively (Fig. 2a). Following a scheme developed recently³² for the reconstruction of the electric and magnetic parts of transverse spin, we used a spherical silicon nanoparticle of diameter $d = 168$ nm as a local probe in the focal volume. The NA of the collection MO₂ was considerably larger than 1 to access the angular range above the critical angle, which is required for the applied reconstruction technique. We then performed a polarization analysis in the back focal plane (BFP) of

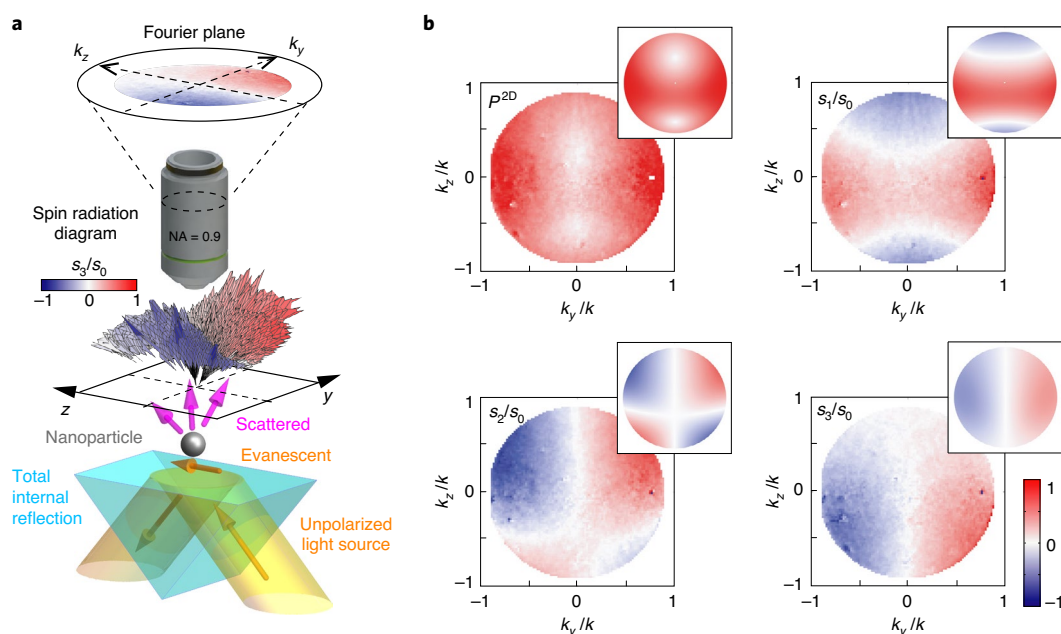


Fig. 3 | Evanescent-wave experiment. **a**, Experimental set-up used to detect the non-zero transverse spin in an evanescent wave from a 2D-unpolarized source. Light from an unpolarized source undergoes total internal reflection, generating an evanescent wave, which is then scattered by a nanoparticle. The scattering from this nanoparticle is collected via a microscope objective. The radiation diagram above the nanoparticle represents the measured P^{2D} (that is, the degree of polarization in different directions) and the colour represents the spin of the far-field radiation given by s_3/s_0 . **b**, Experimentally retrieved and analytically calculated (inset) maps of P^{2D} and normalized Stokes parameters $s_{1,2,3}/s_0$ of the scattered light in every direction of the upper half-space.

MO₂, imaged onto a camera, which allowed us to access the far field of the scattered light. This polarization analysis involved an LC, a linear polarizer and an imaging lens (Fig. 2a). At this stage of the set-up, a single LC is sufficient, because, for reconstruction of the transverse spin, we only need to distinguish between the x and y polarizations. According to the method in ref. ³², the intensities of the x and y components of the scattered field, dependent on the transverse wavevectors $I_{x,y}^{sc}(\mathbf{k}_\perp)$, allow unambiguous reconstruction of both the electric and magnetic field contributions to the transverse spin density, $\mathbf{S}_\perp^{(e)}$ and $\mathbf{S}_\perp^{(m)}$, in the focused field at the location of the particle.

To provide a full map of the transverse electric and magnetic spin densities, $\mathbf{S}_\perp^{(e)}$ and $\mathbf{S}_\perp^{(m)}$, shown in Fig. 2b, we raster-scanned the nanoparticle across the focal plane (over a square area of $1.5 \times 1.5 \mu\text{m}^2$ with a step size of 30 nm) and recorded the polarization-resolved BFP images for each particle position. For each position and polarization, the data were averaged over a time frame of 40 s. The distributions of the transverse spin obtained experimentally are in good agreement with simple theoretical expression (2) with the fitted Rayleigh range $z_R \simeq 527$ nm. We also performed more accurate numerical calculations of the transverse spin densities using vectorial diffraction theory⁴⁴ (which takes into account the finite aperture of the focused beam); these are plotted in the insets of Fig. 2b. In doing so, we adjusted all parameters of the focusing system and the incoming beam to the experimental case. One can see that the experimental results are in excellent agreement with the numerical data.

Importantly, the electric and magnetic spin densities in Fig. 2b exhibit very similar spatial distributions, in agreement with the dual-symmetric nature of the transverse spin for 2D-unpolarized light: $\mathbf{S}_\perp^{(e)} = \mathbf{S}_\perp^{(m)} = \mathbf{S}_\perp/2$ (Supplementary Information). The same feature is present in non-paraxial fields with well-defined helicity¹⁵, such as fields obtained by focusing circularly polarized input light¹⁵. However, in our case of an unpolarized source, the helicity and longitudinal spin vanish. Note also that the change in the 3D degree

of polarization upon focusing^{40,41} is small: $\delta P^{3D} \simeq \tilde{r}^2/4 \simeq 0.036$, where we used $r \simeq 200$ nm, corresponding to the maximum of the spin density in Fig. 2b (Supplementary Information).

Evanescent-wave experiment

To measure the transverse spin of a 2D-unpolarized evanescent wave, the total internal reflection of collimated far-field light coming from an unpolarized tungsten lamp was employed. To generate the evanescent wave, a BK7 glass prism (Thorlabs, refractive index $n = 1.51$ at the wavelength $\lambda = 600$ nm) was illuminated by an unpolarized tungsten lamp of wavelength 500–800 nm. The angle of incidence was measured to be 49° , which changed to 47° following refraction when entering the right-angle prism. This is above the critical angle of 41° , producing total internal reflection and an evanescent wave with $\kappa/k_z \simeq 0.43$ above the glass. Such an evanescent wave has noticeable transverse spin (4) and negligible change in the 3D degree of polarization: $\delta P^{3D} \simeq 0.75(\kappa/k_z)^4 \simeq 0.026$ (neglecting the anisotropy of the Fresnel coefficients, Supplementary Information). Akin to the focused-beam experiment, a small nanoparticle acting as a probe for the local field polarization—in this case a gold nanoparticle (diameter $d = 150$ nm, Sigma Aldrich)—was placed in the evanescent field above the prism and the far-field scattered radiation was analysed (Fig. 3a).

The scattered signal from the gold nanoparticle was collected by a $\times 100$ microscope objective with $\text{NA} = 0.9$, allowing us to analyse the scattered light within a very large solid angle. The BFP of the detection objective (Fourier plane) was then imaged onto an imaging spectrometer using a set of relay lenses. The scattered signal was analysed using a linear polarizer and a quarter wave plate to reconstruct the full Stokes parameters of the light scattered from the particle in all directions in the upper half-space (Supplementary Information). Figure 3b shows the results of these measurements, that is, the angular dependences of the normalized Stokes parameters $s_{1,2,3}/s_0$, as well as the 2D degree of polarization, P^{2D} , for the far-field scattering from the nanoparticle.

Note that the gold nanoparticle in this experiment behaves as an electric dipole; that is, it is sensitive to the electric- rather than magnetic-field properties. However, we have already shown that the magnetic field shares the same features in 2D-unpolarized light, so we omit the superscript '(e)'.

The degree of polarization P^{2D} and third Stokes parameter s_3/s_0 in the scattered radiation show that the scattered light becomes partially polarized and acquires opposite-sign spins in the $\pm y$ directions. This is in perfect agreement with the y -directed transverse spin in equation (4) and the well-established fact that this transverse spin in an evanescent field is converted to the usual far-field spin (that is, the third Stokes parameter) upon transverse scattering by a dipole particle^{23–25,27–29,33–35}. The insets in Fig. 3b show the analytically calculated Stokes parameters of the scattered light for an unpolarized $\lambda=600$ nm source. (The patterns depend very weakly on wavelength, so they are almost constant within the whole 500–800-nm range.) The analytical calculation was performed by matching the experimental parameters (angle of incidence, type of glass, particle diameter and material), including the total internal reflection of the incident beam, the particle modelled as a point dipole, and the subsequent scattering of the particle (taking into account the effects of the surface reflections; Supplementary Information). Very good agreement between the theory and experiment can be seen.

Conclusions

We have shown that pure redirection of wavevectors can generate non-zero spin angular momentum in initially completely 2D-unpolarized paraxial light. This surprising result establishes an important link between two areas of research: 3D polarization in non-paraxial fields^{4–12,40,41} and transverse spin^{17–39}. The direct relation between the redirection of wavevectors and the appearance of spin points to the fundamental spin–orbit interaction origin of this phenomenon³⁴. We have provided theoretical calculations and two sets of experimental measurements for the transverse spin generated upon tight focusing and total internal reflection (that is, generation of an evanescent wave) of unpolarized paraxial light. All these results use well-established methods for spin calculations and measurements, and are in perfect mutual agreement.

Our work has revealed one more exceptional feature of transverse spin. Together with other properties found previously, we can conclude that transverse spin is not just 'one of the components of spin angular momentum density', but rather a separate physical entity whose main features are completely different from those of the usual polarization-controlled longitudinal spin of paraxial light or photons. As such, the transverse spin can offer novel phenomena and applications in angular-momentum and polarization optics. The remarkable 'spin–momentum locking' associated with the transverse spin has already found promising applications for highly efficient spin–direction couplers^{22–25,27–29,33–36}. The present study opens an avenue for the use of spin from unpolarized and incoherent sources. It also sheds light onto the appearance of non-zero local spin in non-paraxial sound waves^{36–38}, which do not feature a polarization degree of freedom in the paraxial regime and correspond to spin-0 quantum particles (phonons).

Online content

Any methods, additional references, Nature Research reporting summaries, source data, extended data, supplementary information, acknowledgements, peer review information; details of author contributions and competing interests; and statements of data and code availability are available at <https://doi.org/10.1038/s41566-020-00733-3>.

Received: 6 April 2020; Accepted: 28 October 2020;

Published online: 21 December 2020

References

- Azzam, R. M. A. & Bashara, N. M. *Ellipsometry and Polarized Light* (North-Holland, 1977).
- Berestetskii, V. B., Lifshitz, E. M. & Pitaevskii, L. P. *Quantum Electrodynamics* (Pergamon, 1982).
- Novotny, L. & Hecht, B. *Principles of Nano-Optics* (Cambridge Univ. Press, 2012).
- Carozzi, T., Karlsson, R. & Bergman, J. Parameters characterizing electromagnetic wave polarization. *Phys. Rev. E* **61**, 2024–2028 (2000).
- Setälä, T., Shevchenko, A., Kaivola, M. & Friberg, A. T. Degree of polarization for optical near fields. *Phys. Rev. E* **66**, 016615 (2002).
- Dennis, M. R. Geometric interpretation of the three-dimensional coherence matrix for nonparaxial polarization. *J. Opt. A Pure Appl. Opt.* **6**, S26–S31 (2004).
- Ellis, J. & Dogariu, A. Optical polarimetry of random fields. *Phys. Rev. Lett.* **95**, 203905 (2005).
- Gil, J. J. Polarimetric characterization of light and media. *Eur. Phys. J. Appl. Phys.* **40**, 1–47 (2007).
- Sheppard, C. J. R. Jones and Stokes parameters for polarization in three dimensions. *Phys. Rev. A* **90**, 023809 (2014).
- Brosseau, C. & Dogariu, A. Symmetry properties and polarization descriptors for an arbitrary electromagnetic wavefield. *Prog. Opt.* **49**, 315–380 (2006).
- Petrucelli, J. C., Moore, N. J. & Alonso, M. A. Two methods for modeling the propagation of the coherence and polarization properties of nonparaxial fields. *Opt. Commun.* **283**, 4457–4466 (2010).
- Alonso, M. A. Geometric descriptions for the polarization for nonparaxial optical fields: a tutorial. Preprint at <https://arxiv.org/abs/2008.02720> (2020).
- Enk, S. Jvan & Nienhuis, G. Spin and orbital angular momentum of photons. *Europhys. Lett.* **25**, 497–501 (1994).
- Berry, M. V. & Dennis, M. R. Polarization singularities in isotropic random vector waves. *Proc. R. Soc. Lond. A* **457**, 141–155 (2001).
- Bliokh, K. Y., Alonso, M. A., Ostrovskaya, E. A. & Aiello, A. Angular momenta and spin–orbit interaction of nonparaxial light in free space. *Phys. Rev. A* **82**, 063825 (2010).
- Cameron, R. P., Barnett, S. M. & Yao, A. M. Optical helicity, optical spin and related quantities in electromagnetic theory. *New J. Phys.* **14**, 053050 (2012).
- Bliokh, K. Y. & Nori, F. Transverse and longitudinal angular momenta of light. *Phys. Rep.* **592**, 1–38 (2015).
- Bliokh, K. Y. & Nori, F. Transverse spin of a surface polariton. *Phys. Rev. A* **85**, 061801 (2012).
- Banzer, P. et al. The photonic wheel—demonstration of a state of light with purely transverse angular momentum. *J. Eur. Opt. Soc.* **8**, 13032 (2013).
- Bliokh, K. Y., Bekshaev, A. Y. & Nori, F. Extraordinary momentum and spin in evanescent waves. *Nat. Commun.* **5**, 3300 (2014).
- Canaguier-Durand, A. & Genet, C. Transverse spinning of a sphere in a plasmonic field. *Phys. Rev. A* **89**, 033841 (2014).
- Neugebauer, M., Bauer, T., Banzer, P. & Leuchs, G. Polarization tailored light driven directional optical nanobeacon. *Nano Lett.* **14**, 2546–2551 (2014).
- Rodríguez-Fortuño, F. J. et al. Near-field interference for the unidirectional excitation of electromagnetic guided modes. *Science* **340**, 328–330 (2013).
- Petersen, J., Volz, J. & Rauschenbeutel, A. Chiral nanophotonic waveguide interface based on spin–orbit interaction of light. *Science* **346**, 67–71 (2014).
- O'Connor, D. et al. Spin–orbit coupling in surface plasmon scattering by nanostructures. *Nat. Commun.* **5**, 5327 (2014).
- Neugebauer, M., Bauer, T., Aiello, A. & Banzer, P. Measuring the transverse spin density of light. *Phys. Rev. Lett.* **114**, 063901 (2015).
- le Feber, B., Rotenberg, N. & Kuipers, L. Nanophotonic control of circular dipole emission. *Nat. Commun.* **6**, 6695 (2015).
- Lefier, Y. & Grosjean, T. Unidirectional sub-diffraction waveguiding based on optical spin–orbit coupling in subwavelength plasmonic waveguides. *Opt. Lett.* **40**, 2890–2893 (2015).
- Bliokh, K. Y., Smirnova, D. & Nori, F. Quantum spin Hall effect of light. *Science* **348**, 1448–1451 (2015).
- Bekshaev, A. Y., Bliokh, K. Y. & Nori, F. Transverse spin and momentum in two-wave interference. *Phys. Rev. X* **5**, 011039 (2015).
- Bauer, T., Neugebauer, M., Leuchs, G. & Banzer, P. Optical polarization Möbius strips and points of purely transverse spin density. *Phys. Rev. Lett.* **117**, 013601 (2016).
- Neugebauer, M., Eismann, J. S., Bauer, T. & Banzer, P. Magnetic and electric transverse spin density of spatially confined light. *Phys. Rev. X* **8**, 021042 (2018).
- Aiello, A., Banzer, P., Neugebauer, M. & Leuchs, G. From transverse angular momentum to photonic wheels. *Nat. Photon.* **9**, 789–795 (2015).
- Bliokh, K. Y., Rodríguez-Fortuño, F. J., Nori, F. & Zayats, A. V. Spin–orbit interactions of light. *Nat. Photon.* **9**, 796–808 (2015).
- Lodahl, P. et al. Chiral quantum optics. *Nature* **541**, 473–480 (2017).
- Shi, C. et al. Observation of acoustic spin. *Nat. Sci. Rev.* **6**, 707–712 (2019).
- Bliokh, K. Y. & Nori, F. Spin and orbital angular momenta of acoustic beams. *Phys. Rev. B* **99**, 174310 (2019).

38. Toftul, I. D., Bliokh, K. Y., Petrov, M. I. & Nori, F. Acoustic radiation force and torque on small particles as measures of the canonical momentum and spin densities. *Phys. Rev. Lett.* **123**, 183901 (2019).
39. Golat, S., Lim, E. A. & Rodríguez-Fortuño, F. J. Evanescent gravitational waves. *Phys. Rev. D* **101**, 084046 (2020).
40. Lindfors, K., Friberg, A. T., Setälä, T. & Kaivola, M. Degree of polarization in tightly focused optical fields. *J. Opt. Soc. Am. A* **22**, 561–568 (2005).
41. Lindfors, K. et al. Local polarization of tightly focused unpolarized light. *Nat. Photon.* **1**, 228–231 (2007).
42. Bliokh, K. Y., Bekshaev, A. Y. & Nori, F. Dual electromagnetism: helicity, spin, momentum and angular momentum. *New J. Phys.* **15**, 033026 (2013).
43. Banzer, P., Peschel, U., Quabis, S. & Leuchs, G. On the experimental investigation of the electric and magnetic response of a single nano-structure. *Opt. Express* **18**, 10905–10923 (2010).
44. Richards, B. & Wolf, E. Electromagnetic diffraction in optical systems. II. Structure of the image field in an aplanatic system. *Proc. R. Soc. Lond. A* **253**, 358–379 (1959).
45. Eismann, J. S., Banzer, P. & Neugebauer, M. Spin–orbit coupling affecting the evolution of transverse spin. *Phys. Rev. Res.* **1**, 033143 (2019).

Publisher's note Springer Nature remains neutral with regard to jurisdictional claims in published maps and institutional affiliations.

© The Author(s), under exclusive licence to Springer Nature Limited 2020

Data availability

The data that support the plots within this paper and other findings of this study are available from the corresponding authors upon reasonable request.

Code availability

The codes that support the calculations and plots within this paper and other findings of this study are available from the corresponding authors upon reasonable request.

Acknowledgements

We acknowledge the help of U. Mick with the fabrication of samples for the focused-beam experiment. This work was partially supported by the European Research Council (Starting Grant ERC-2016-STG-714151-PSINFONI and iCOMM project no. 789340), EPSRC (UK), the Excellence Initiative of Aix Marseille University—A*MIDEX, a French 'Investissements d'Avenir' programme, NTT Research, the Army Research Office (ARO; grant no. W911NF-18-1-0358), Japan Science and Technology Agency (JST; via CREST grant no. JPMJCR1676), Japan Society for the Promotion of Science (JSPS; JSPS-RFBR grant no. 17-52-50023 and KAKENHI grant no. JP20H00134), the Foundational Questions Institute Fund (FQXi; grant no. FQXi-IAF19-06) and a donor advised fund of the Silicon Valley Community Foundation.

Author contributions

K.Y.B. conceived the idea for this research, made theoretical calculations with input from M.A.A. and prepared the manuscript with input from all the authors. Focused-beam experiment: P.B. and J.S.E. developed the idea of the experiment; J.S.E. performed the experiment; J.S.E. and P.B. performed the data processing; J.S.E. and P.B. wrote the corresponding part of the manuscript. Evanescent-wave experiment: F.J.R.-F., D.J.R., L.H.N. and A.V.Z. developed the idea of the experiment; D.J.R. and L.H.N. designed and performed the experiment; F.J.R.-F. performed theoretical modelling; D.J.R. and F.J.R.-F. performed data processing; D.J.R. fabricated the samples; F.J.R.-F., D.J.R., L.H.N. and A.V.Z. wrote the related part of the manuscript.

Competing interests

The authors declare no competing interests.

Additional information

Supplementary information is available for this paper at <https://doi.org/10.1038/s41566-020-00733-3>.

Correspondence and requests for materials should be addressed to P.B., A.V.Z. or K.Y.B.

Peer review information *Nature Photonics* thanks Lorenzo Marrucci and the other, anonymous, reviewer(s) for their contribution to the peer review of this work.

Reprints and permissions information is available at www.nature.com/reprints.